Study of the Molecular Orientation Heterogeneity in Polypropylene Injection-Molded Parts by Raman Spectroscopy

J. Martin, S. Margueron, M. Fontana, M. Cochez, P. Bourson

Laboratoire Matériaux Optiques, Photonique et Systèmes,

Université Paul-Verlaine de Metz, UMR-CNRS 7132, Supélec, 57070 Metz, France

Study of the Molecular Orientation Heterogeneity in Polypropylene Injection-Molded Parts by Raman Spectroscopy

J. Martin, S. Margueron, M. Fontana, M. Cochez, P. Bourson

Laboratoire Matériaux Optiques, Photonique et Systèmes,

Université Paul-Verlaine de Metz, UMR-CNRS 7132, Supélec, 57070 Metz, France

ABSTRACT

Polarized Raman micro-spectroscopy has been used to study oriented-skin layers induced in injection-molded isotactic polypropylene (iPP) parts. A method based on the intensity sensitivity of several Raman bands to laser light polarization was employed to estimate the degree of molecular orientation in iPP. The skin-core molecular orientation heterogeneity in injection-molded iPP is then evaluated via two different experimental methods. Results show that an in-depth profile using micro-Raman confocal technique is as valuable as an edge profile performed on a sample cross-section because both are correlated with optical microscopy measurements. Both Raman measurements are in good agreement with optical microscopy measurements. The skin development was found to be narrowly related to the shear strain rate at the mold walls.

INTRODUCTION

The mechanical response of the semi-crystalline polymers is strongly dependent on the semi-crystalline microstructure which are induced by the rheological processing conditions such as injection melt temperature T_{inj} (° C), cooling mold temperature T_w (° C), flow rate Q_{inj} ($mm^3.s^{-1}$) and mold geometry [1-4]. Injection-molding is a well-known processing method to produce plastic parts for engineering applications. During the process, a hot polymer melt is forced to flow into the cavity of a mold under complex thermo-mechanical conditions characterized by a high cooling rate and an important shear field, especially at the walls of the mold. Thus, the final semi-crystalline microstructure of the injection-molded plastic parts is far from being homogeneous and isotropic. This microstructure is widely reported in the literature and shows a hierarchy of macromolecular arrangements and a through-the-thickness morphological gradient [5,6]. In a simple description it consists of a multilayered structure, e.g., skin and core, parallel to the surface of the mold. The skin morphology exhibits a highly-oriented shish-kebab like structure along the injection direction while radial spherulites are observed in the core region [7]. Individual properties and relative importance of each layer determine the mechanical end-use properties of the molded parts [8-10]. Few numerical studies tempt to simulate the solidification and the resulting mechanical properties of injection-molded parts [11,12].

Nowadays, there is an increasing demand by plastic transformers of new developments in micro-structural control methods in order to monitor processes in real-time with insurance of quality, reproducibility and rapidity [13,14]. Typically, analytical techniques such as light diffraction [15], Differential Scanning Calorimetry

(DSC) [16], X-ray scattering [17], Scanning Electron Microscopy [18], Infra-Red absorption [19] and Nuclear Magnetic Resonance [20] are suitable for polymer morphological analysis but require long and destructive sampling procedure and provide only particular morphological informations. In this paper we propose the use of the Raman spectroscopy to characterize the molecular orientation of injection-molded isotactic polypropylene (iPP) parts.

Raman spectroscopy is a well-suitable technique to study the vibrational characteristics of polymer molecules. This technique is an ideal tool for polymer analysis especially for the study of saturated and unsaturated C-C bonds [21,22] and provides the analysis of molecular species at different scales, from the chemical bond up to the conformational architecture. The Raman spectrum of iPP has been the object of several investigations, and the assignment of the Raman bands are rather well established [23-25]. The development of confocal technique associated with classical Raman spectrometer has considerably improved spatial resolutions in particular axial resolution. It consists on placing a variable aperture at the focal image plan in order to analyze only the light scattered from the interaction focal volume [26].

In this paper, using the polarized Raman micro-spectroscopy, we characterize the molecular orientation heterogeneity in injection-molded iPP parts. We particularly point out the skin-core laminated structure and show how it may be affected with rheological conditions induced by mold geometry variations.

EXPERIMENTAL PROCEDURES

Injection Molded Parts

The iPP resin granules manufactured by Repsol YPF were used to prepare samples. Four rectangular plates were molded by injection using an Arburg 250-75 machine under T_{inj} = 200 °C as the heating temperature, T_w = 25 °C as the cooling temperature and P = 10 bars as the pressure. As shown in the Fig. 1, the specimen length L and width w were kept constant to 32 and 16 mm respectively. The thicknesses of the plates were h_1 = 0.5, h_2 = 1, h_3 = 2 and h_4 = 4 mm. The injection direction is parallel to the width w along Z-axis.

Especially for molecular orientation assignment, one specific rectangular dumbbell-shape test specimens with overall dimensions of 34 x 10 x 4 mm^3 was also prepared by injection molding and then uniaxially stretched. The median region is reduced to 9 mm in order to localize necking in this predetermined zone. Nominal strain was calculated from the ratio of the increment of the length between clamps to the initial gauge length. Nominal tensile stress was determined from dividing the tensile load by the initial cross section. Mechanical tests were performed at 25 °C under a constant cross-head speed of about 5 $mm.min^{-1}$. A nominal deformation of ε_N = 200 % is achieved in order to enhance molecular orientation along the stretching direction. The injected material has an average crystallinity index of 53-55 %, as determined by DSC (Perkin-Elmer DSC4 calorimeter) with a major proportion of the monoclinic α-crystal form (95 % in weight). The influence of the hexagonal β-crystal form is not taking into account in this work. The iPP used has a melting point T_m near to 165 °C and a crystallization point T_c near to 143 °C.

Raman Spectroscopy

All Raman scattering measurements are carried out on a LabRam micro-spectrometer developed by Horiba Jobin Yvon (Lille, France). A Helium-Neon laser emitting a 633 nm exciting line is used. The system is equipped with a liquid nitrogen cooled, 2000 x 256 pixels CCD detector (Synapse, Horiba Jobin Yvon). All spectra are recorded in back-scattered geometry using an 1800 grooves.mm^{-1} centered at 950 cm^{-1} as the diffraction grating. A spectral resolution of about 1.2 cm^{-1} is achieved. The useful spectrum under consideration is ranging from 750 cm^{-1} to 1100 cm^{-1}. Both the incident and scattered lights are collected through an Olympus confocal microscope (x 100 objective lens, total magnification x 1000, numerical aperture NA = 0.9). In this configuration, the lateral (along **x** and **y**-direction) and the axial (along **z**–direction) space resolution are about of 1.1 µm and 1,9 µm respectively. When the laser beam is focus onto the sample, the illumination power is about of 16 mW. Rayleigh scattered light is block by using a holographic Notch filter. A set of two polarisers is also installed on the spectrometer and offers the possibility to polarize both the incident and the scattered radiation independently. All Spectra are recorded with the Labspec® acquisition software developed by Horiba Jobin Yvon (Lille, France). Acquisition time is equal to 20 s and final spectrum is an average of ten spectra. A personal fitting least-square procedure based on a Lorentzian function adjustment is used to process spectral data and decompose the bands into their wavenumber position, absolute intensity, full-width at half maximum and integrated intensity. In this study, we just take into account of the integrated intensity.

Molecular Orientation Assignments

In Fig. 2, we define a coordinate system referred to the sample (O, X, Y, Z). Spectra were recorded on the necked area of the uniaxially drawn dumbbell-shape test specimen. According to Porto's nomenclature [27], two perpendicular polarization geometries were used: X(ZZ)X and X(YY)X respectively parallel and perpendicular to the stretching direction. To explore these two polarization configurations, we used a computer-controlled rotational device permitting to turn the sample by remaining one polarization configuration constant.

Skin Layer Profiles

To characterize molecular orientation heterogeneity through the thickness in the rectangular plate specimens, two different experimental methods were employed. An edge profile was undertaken on the cross-section of one plate specimen from the surface to -600 µm distance. The cross-sections were obtained by carefully cutting plates into two equal parts along specimen width *w* and then manually polishing with grinding paper of sequentially lower grain sizes. Then an in-depth profile through specimen thickness from the surface to -600 µm depth was performed with a confocal microscope system which is coupled with our Raman spectrometer. The pinhole was adjusted to 100 µm diameter which offers a sufficient axial resolution up to -600 µm in depth. For both experimental methods used, the laser radiation polarization was maintained parallel to injection direction along Z-axis. In order to correlate our measurements, optical microscopy using polarized visible radiation is applied on microtomic slices. Measure of skin thickness is also possible on the optical micrographs recorded.

RESULTS AND DISCUSSION

Molecular Orientation Assignments

The two different scattering configurations defined previously allow the determination of the Raman bands, which are sensitive to chains orientation. Two spectral regions are particularly examined and carefully fitted to a Lorentzian profile. The first range around 820 cm^{-1} is structured into three separated bands located at 809, 835, and 841 cm^{-1}. The 809 and 841 cm^{-1} correspond to the C-C skeletal symmetric stretching mode v_s(C-C) and to the CH_2 lateral alkyl rocking mode $r(CH_2)$ respectively [23-25]. Both are referred to the 3_1 helical chain conformation or crystalline phase. It is noted that the 835 cm^{-1} band related to the C-C skeletal symmetric stretching mode v_s(C-C) in non-helical chain conformation is not considered in the present discussion. The second range around 980 cm^{-1} shows two separate bands at 973 and 998 cm^{-1}. The 973 cm^{-1} band has been assigned to the C-C skeletal asymmetric stretching mode v_{as}(C-C) whereas the 998 cm^{-1} band has been referred to the CH_3 lateral alkyl rocking mode $r(CH_3)$. Both are also referred to the 3_1 helical chain conformation or crystalline phase. The vibrational assignments of the Raman bands considered are given in Table 1.

Fig. 3 (a) and (b) shows the X(YY)X and X(ZZ)X spectra recorded on an unstretched (ε_N=0 %) and a stretched specimen (ε_N=200 %) for two wavenumber ranges. By remaining laser light polarization parallel to the tensile direction (X(ZZ)X), bands at 809 cm^{-1} and 973 cm^{-1} are dominant while bands located at 841 cm^{-1} and 998 cm^{-1} have a weak intensity. This is amplified with the pre-oriented stretched specimen. On the contrary, by remaining laser light polarization perpendicular to the

tensile direction (X(YY)X), bands at 809 cm^{-1} and 973 cm^{-1} are weak while bands at 841 cm^{-1} and 998 cm^{-1} have a dominant intensity. This is also amplified with the pre-oriented stretched specimen.

These observations can be understood by means of the molecular vibration associated to each Raman band. In the uniaxially pre-oriented stretched sample, skeletal backbone C-C are preferentially oriented parallel to the stretching direction whereas lateral alkyl groups are preferentially oriented perpendicular to the stretching direction. Thus, when the polarization is parallel to the stretching direction, Raman scattering comes principally from C-C backbones which explains the high intensity of bands at 809 and 973 cm^{-1}. On the contrary, when polarization is kept perpendicular to the stretching direction, Raman scattering comes principally from lateral alkyl groups CH_2 and CH_3 which explains the high intensity of bands at 841 and 998 cm^{-1}. The use of the two ratio J(809)/J(841) and J(973)/J(998) is therefore a valuable tool to characterize molecular orientation heterogeneity induced in iPP injection-molded parts. Table 2 resumes the ratio for the unstretched and the pre-oriented stretched specimens taken in two perpendicular laser light polarizations.

Edge and In-Depth Profiles

Edge profiles were performed on the cross-sections of the injection-molded rectangular plates. Keeping the laser light polarization toward the injection direction Z, the ratio of integrated intensity defined previously J(809)/J(841) and J(973)/J(998) are used to discriminate preferential molecular orientation in the skin layer. Theses ratio are expected to predominate in the skin region as in the core region. Fig. 4 shows the

evolution of the ratio along the edge profile only for the plate with a thickness of h_4 = 4 mm. As expected, the ratios are much stronger on close surface as in core region and continuously decrease toward the core region. In the core region, the ratios show any variation. Thus the molecular orientation is anisotropic in the skin region. Chains are preferentially oriented along the injection direction and refer to an oriented shish-kebab structure. On the contrary, in the core region the molecular orientation is isotropic and refers to a spherulitic structure [7-10]. The decrease of the ratio observed between the extreme surface and the core region is related to an increase of the spherulitic proportion from the surface to the core region. A skin thickness e_{skin} can be directly determined from the Fig. 4. Thus a skin layer thickness can be evidenced as $e^{h_4}_{skin}$ = 160 µm. Fig. 5 presents an optical micrograph obtained from the cross-section of the thickest plate (h_4=4mm) and skin thickness found has a close similarity as the Raman measurements. Identical investigations were performed on the others rectangular plates and the skin thicknesses determined for each plate are summarized in Table 3.

In-depth profiles were performed through the thickness with maintaining the laser light polarization toward the injection direction along Z-axis. Fig. 6 shows the evolution of the ratio J(973)/J(998) through the thickness for the four different injection-molded plates considered in this study. It is noted that the ratio J(809)/J(841) exhibits the same variations. As remarked previously, close to the surface, the ratio is larger than in internal region. It corresponds respectively to the skin and core regions. From the Fig. 6, it is also possible to determine a skin layer thickness e_{skin} which is arbitrary limited by the point of inflection of the skin-to-core transition. Table 3 summarizes the skin layer thicknesses e_{skin} versus plate thicknesses h determined from

edge and in-depth Raman profiles. Any ratio variation can be observed for the h_1 = 0.5 mm plate thickness. Due to the fact that the thickness is very thin, the entire plate is highly oriented and can be considered as a skin layer. Fig. 7 shows that the skin layer thicknesses measured by the edge and the in-depth method are in good agreement with optical microscopy experiments. This result proves the usefulness of confocal depth analysis from 0 to -600 µm in estimating skin-core laminated structure induced in injection-molded parts.

Rheological Aspect

From Table 3, it is observed that the skin layer thickness increases with the decreasing of the plate thickness. Fig. 8 illustrates this behavior in representing the skin layer thicknesses e_{skin} previously determined in function of the thickness h of the plates used. It is worth to mention that the plate thickness h correspond also to the thickness of the mold cavity. Thus the skin thickness varies with the mold geometry as $1/h^2$. A comparison can be made with the well-known rheological model which described the shear strain rate $\dot{\gamma}_{wall}$ at the wall of the mold for a non-Newtonian flow through a rectangular channel [28-29]:

$$\dot{\gamma}_{wall} = \frac{2.Q_{inj}}{w.h^2} \qquad (1)$$

Equation shows that shear strain rate $\dot{\gamma}_{wall}$ at the wall of the mold is proportional to the flow rate Q_{inj} and inversely proportional to the width w and the thickness h of the mold cavity. Especially, $\dot{\gamma}_{wall}$ and e_{skin} vary similarly with the thickness of the mold cavity as $1/h^2$ as it can be seen in Fig. 8. In other words, skin layer

thickness is directly related to the shear strain rate at the wall which depends on the mold geometry. Thin plates experience much stronger melt-shear during the injection-molding process. It must be pointed out that for a certain sample thickness, the skin layer becomes higher than the sample thickness and we can consider that the entire sample is highly oriented.

CONCLUSIONS

By using two perpendicular laser light polarizations on a highly oriented sample, we have selected specific Raman bands which are sensitive to the molecular orientation. We show that intensity ratio J(809)/J(841) and J(973)/J(998) can be used as the Raman assignments of the molecular orientation of isotactic polypropylene chains. Taking into account of this result, polarized Raman spectroscopy coupled with the confocal technique was successfully used to study the molecular orientation heterogeneity into injection-molded iPP parts. Especially, the oriented-skin layer thickness was determined and compared with two different experimental ways. In-depth profiles are well-correlated with edge profiles. For the processing window considered, the mold geometry has a great influence on the imposed shear stress level and on the skin development.

ACKNOWLEDGMENTS

The authors are grateful to the engineering researchers from Plate Forme de Technologie Plastinnov (Université Paul-Verlaine de Metz) for valuable help and stimulating discussions all along this study.

REFERENCES

1. P. Zipper, A. Janosi, W. Geymayer, E. Ingolic, and E. Fleischmann, *Polym. Eng. Sci.*, **36**, 467 (1996)

2. J.C. Viana, A.M. Cunha, and N. Billon, *Polym. Int.*, **43**, 159 (1997)

3. J.C. Viana, N. Billon, and A.M. Cunha, *Polym. Eng. Sci*., **44**, 1522 (2004)

4. J.C. Viana, *Polymer*, **46**, 11773 (2005)

5. E.S. Clark, and J.E. Spruiell, *Polym. Eng. Sci*., **16**, 176 (1976)

6. Z. Mencik, and D.R. Fitchmum, *Polym. Sci.: Polym. Phys. Ed.*, **11**, 973 (1973)

7. M. Fujiyama, T. Wakino, and Y. Kawasaki, *Appl. Polym. Sci.*, **35**, 29 (1988)

8. M.R. Kantz, Jr. H. D. Newman, and F.H. Stigale, *Appl. Polym. Sci*., **16**, 1249 (1972)

9. G. Kalay, and M.J. Bevis, *Polym. Sci.*, **35**, 265 (1997)

10. J.C. Viana, A.M. Cunha, and N. Billon, *Polym. Eng. Sci.*, **39**, 1463 (1999)

11. A. Almeida, L. Faria, and R. Febra, *Comput. Methods Appl. Mech. Eng.*, **151**, 163 (1998)

12. W. Michaeli, and H. Keller, *Comput. Mat. Sci.*, **7**, 253 (1996)

13. P.D. Coates, *Polymer processing: in-process measurements*, Pergamon Press, New York (2001)

14. G. Lamberti, and V. Brucato, *Polym. Sci.*, **41**, 998 (2003)

15. J. Schultz, *Polymer materials science*, Prentice-Hill, Englewood Cliffs (1974)

16. U.W. Gedde, *Polymer physics*, Chapman & Hall, London, 158 (1995)

17. A. Turner-Jones, J.M. Aizelwood, and D.R. Beckette, *Makromol. Chem.*, **75**, 134 (1964)

18. M. Aboulfaraj, B. Ulrich, A. Dahoun, and C. G'Sell, *Polymer*, **34**, 4817 (1993)

19. H. Hendus, and G. Schnell, *Kunstoffe*, **51**, 69 (1961)

20. K. Bergmann, *Polym. Bull.*, **5**, 355 (1981)

21. J.M. Hollas, *Modern spectroscopy*, 3rd ed., John Wiley&Sons Ltd, Chichester (1996)

22. J.L. Koenig, *Appl. Spectrosc. Rev.*, **4**, 233 (1971)

23. H. Tadokoro, M. Kobayashi, M. Ukita, K. Yasufuku, and S. Murahashi, *Chem. Phys.*, **42**, 1432 (1965)

24. G.V. Fraser, P.J. Hendra, D.S. Watson, M.J. Gall, H.A. Willis, and M.E.A. Cudby, *Spectrochim. Acta.*, **29**, 1525 (1973)

25. R.M. Khafagy, *Polym. Sci.*, **44**, 2173 (2006)

26. J.M. Chalmers, H.G.M. Edwards, J.S. Lees, D.A. Long, M.W. Mackenzie, and H.A. Willis, *Raman Spectrosc.*, **22**, 613 (1991)

27. T.C. Damen, S.P.S. Porto, and B. Tell, *Phys. Rev.*, **142**, 570 (1966)

28. D.G. Baird, and D.I. Collias, *Polymer processing*, Butterworth-Heinemann, Boston 1995

29. P.W. Zhu, G. Edward, *Polymer*, **45**, 2609 (2004)

FIGURES CAPTIONS

Figure 1: The four rectangular injection-molded plates considered in this study and characterized by different thicknesses *h*: h_1 = 0.5, h_2 = 1, h_3 = 2 and h_4 = 4 mm.

Figure 2: Raman scattering geometry used on a pre-oriented stretched dumbbell-shape specimen. Two perpendicular light polarizations are used: X(ZZ)X and X(YY)X.

Figure 3 : X(ZZ)X and X(YY)X Raman spectra recorded on an unstretched (ε_N=0%) and a pre-oriented stretched dumbbell-shape test specimen (ε_N=200%). Two wavenumber ranges are explored: **(a)** 780 – 870 cm^{-1}, **(b)** 960 – 1010 cm^{-1}.

Figure 4 : Evolution of the ratio J(809)/J(841) **(a)** and J(973)/J(998) **(b)** versus depth for the thickest plate (h_4 = 4 mm) by the edge investigation method.

Figure 5 : Optical micrograph performed on the cross-section of the thickest plate (h_4 = 4 mm)

Figure 6 : Evolution of the ratio J(973)/J(998) versus depth for all the rectangular plates by the in-depth investigation method.

Figure 7 : Correlation between the skin thicknesses determined by the in-depth and the edge investigation methods.

Figure 8 : Influence of the mold geometry on the skin thickness.

TABLE 1. Vibrational assignments of the bands considered between 750 cm^{-1} and 1100 cm^{-1}. Ref. [23]

Position (cm-1)	**Vibrational mode**	**Conformation**	**Phase**
809	ν_s(C-C)	Helical	Crystalline
835	ν_s(C-C)	Non-Helical	Amorphous
841	*r*(CH2)	Helical	Crystalline
973	ν_{as}(C-C)	Helical	Crystalline
998	*r*(CH3)	Helical	Crystalline

ν_s, symmetric stretching; ν_{as}, asymmetric stretching; r, rocking

TABLE 2. Ratio J(809)/J(841) and J(973)/J(998) calculated for an unstretched (ε_N=0%) and a pre-oriented stretched dumbbell-shape test specimen (ε_N=200%) in two perpendicular light polarizations X(ZZ)X and X(YY)X.

	J(809)/J(841)		**J(973)/J(998)**	
ε_N (%)	X(ZZ)X	X(YY)X	X(ZZ)X	X(YY)X
0	3.8	0.64	7.2	0.61
200	9.1	0.46	19	0.43

TABLE 3. Skin thickness e_{skin} determined by edge and in-depth Raman profiles for the four rectangular plates.

Sample	**Thickness *h* (mm)**	e_{skin} **(µm)**		
		Edge measurements	In-depth measurements	Microscopy measurements
h_1	0.5	500	500	500
h_2	1	490	480	490
h_3	2	350	320	340
h_4	4	160	150	155

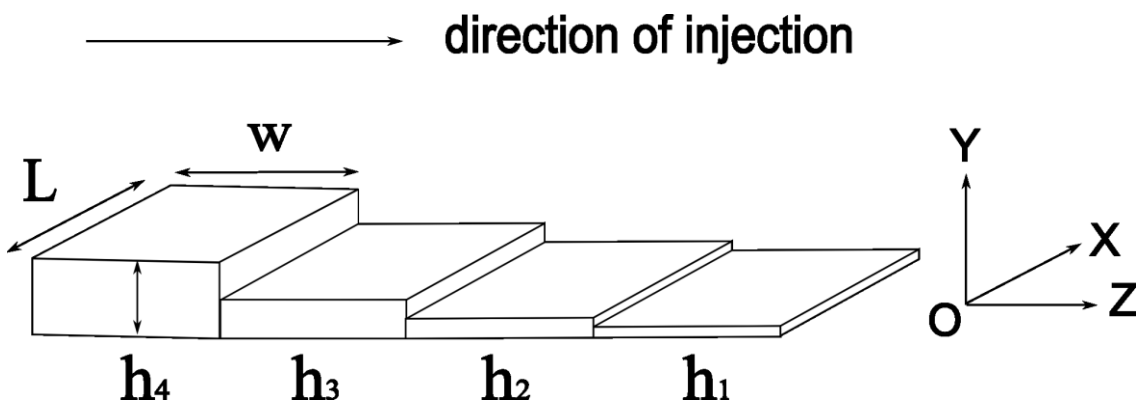

Figure 1 : The four rectangular injection-molded plates considered in this study and characterized by different thicknesses *h*: h_1 = 0.5, h_2 = 1, h_3 = 2 and h_4 = 4 mm.

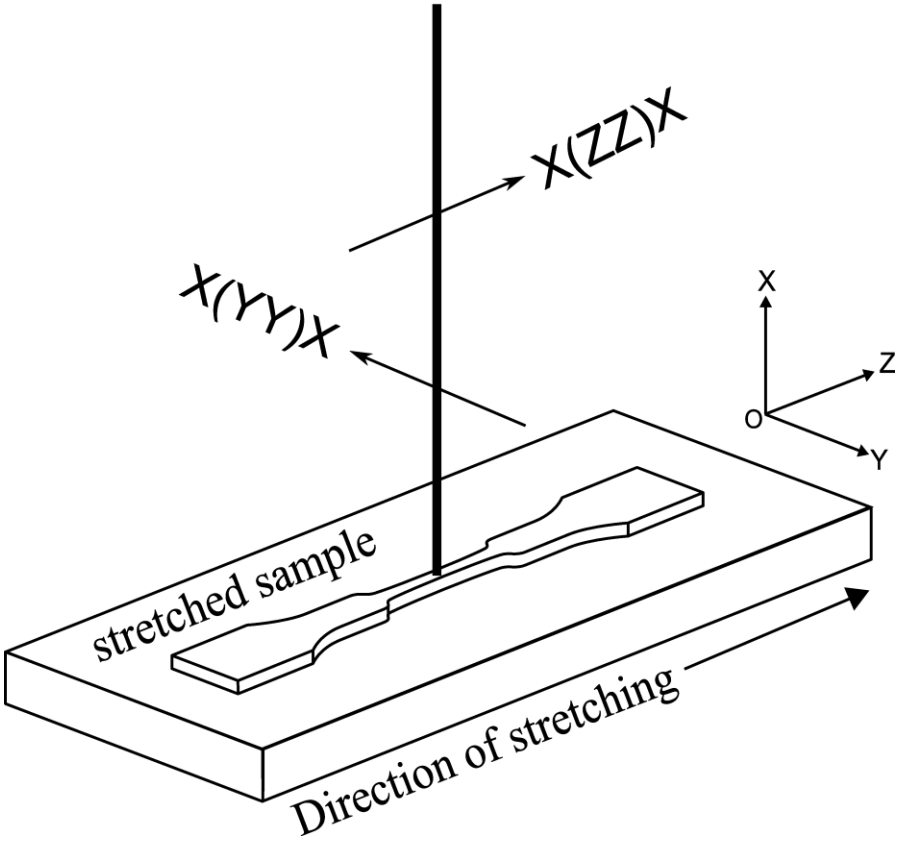

Figure 2: Raman scattering geometry used on a pre-oriented stretched dumbbell-shape specimen. Two perpendicular light polarizations are used: X(ZZ)X and X(YY)X.

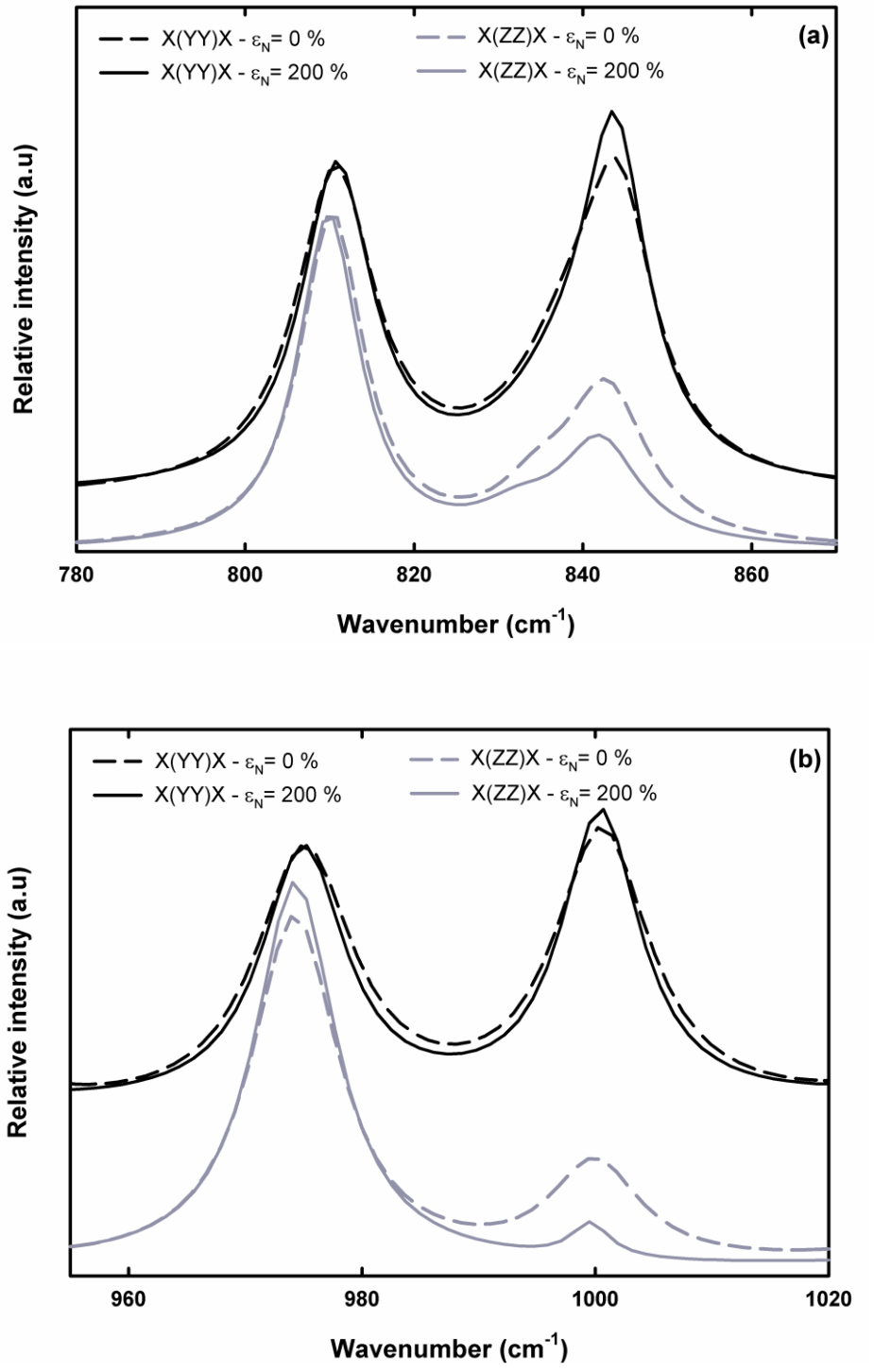

Figure 3 : X(ZZ)X and X(YY)X Raman spectra recorded on an unstretched (ε_N=0%) and a pre-oriented stretched dumbbell-shape test specimen (ε_N=200%). Two wavenumber ranges are explored: **(a)** 780 – 870 cm^{-1}, **(b)** 960 – 1010 cm^{-1}.

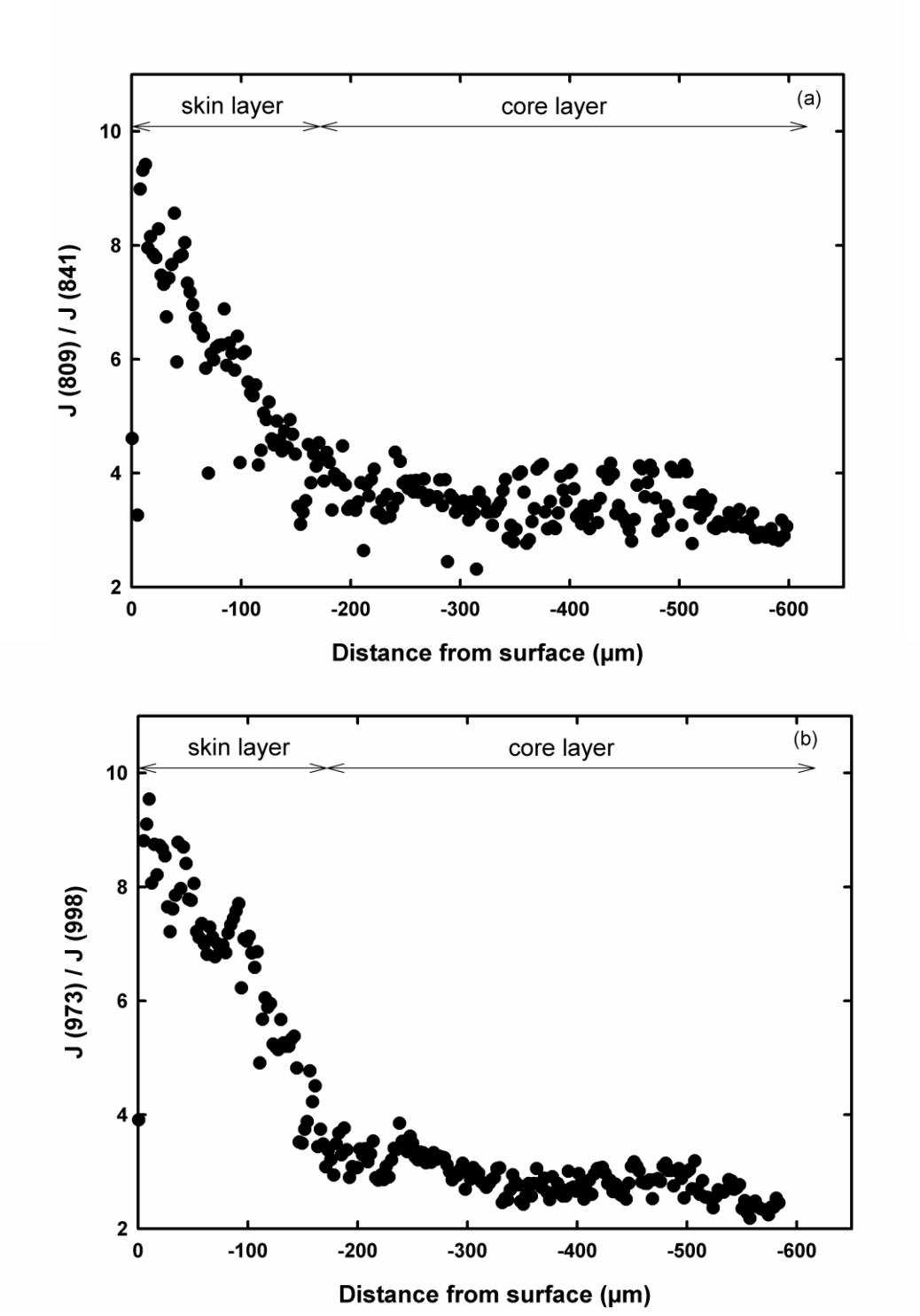

Figure 4 : Evolution of the ratio J(809)/J(841) **(a)** and J(973)/J(998) **(b)** versus depth for the thickest plate (h_4 = 4 mm) by the edge investigation method.

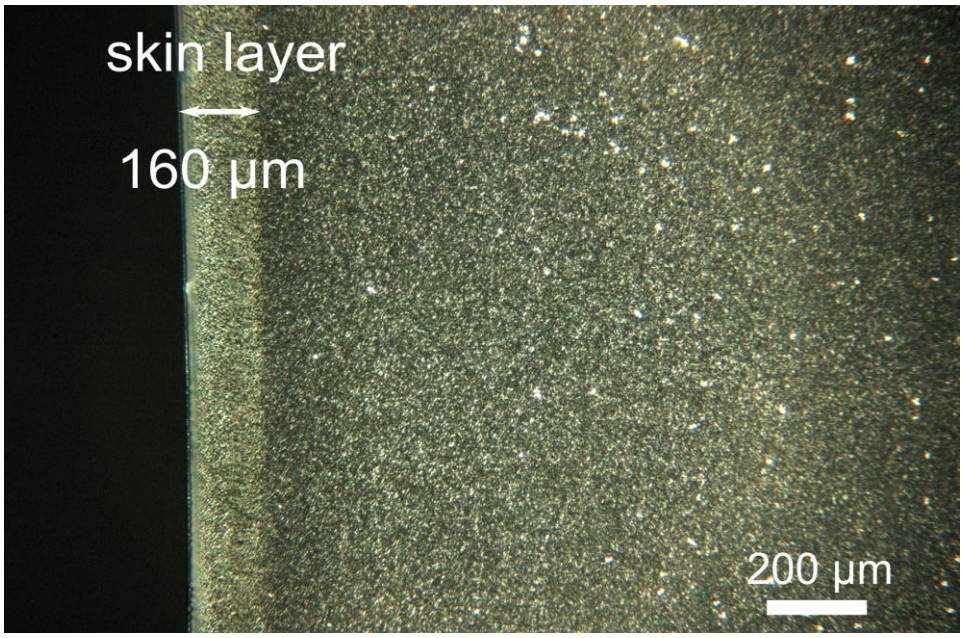

Figure 5 : Optical micrograph performed on the cross-section of the thickest plate (h_4 = 4 mm)

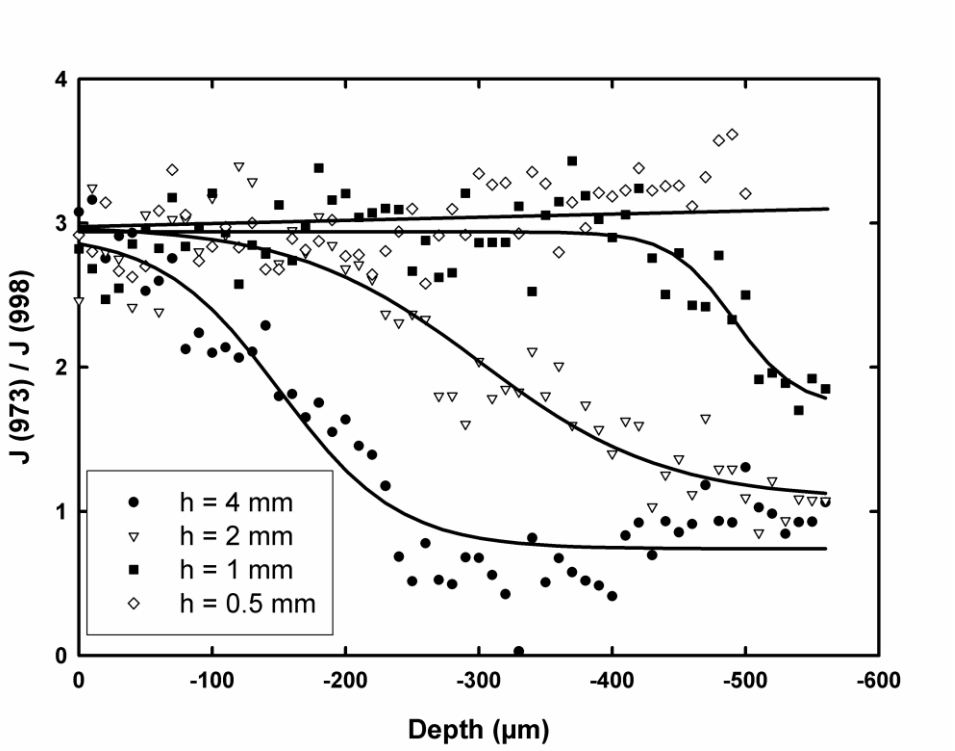

Figure 6 : Evolution of the ratio J(973)/J(998) versus depth for all the rectangular plates by the in-depth investigation method.

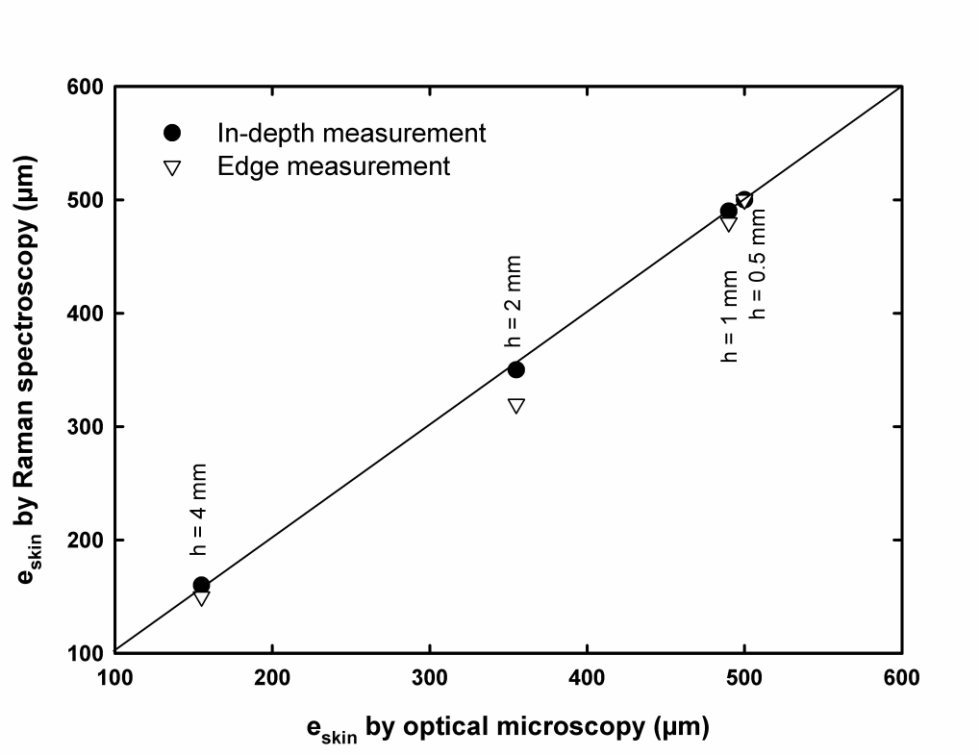

Figure 7 : Correlation between the skin thicknesses determined by the in-depth and the edge investigation methods.

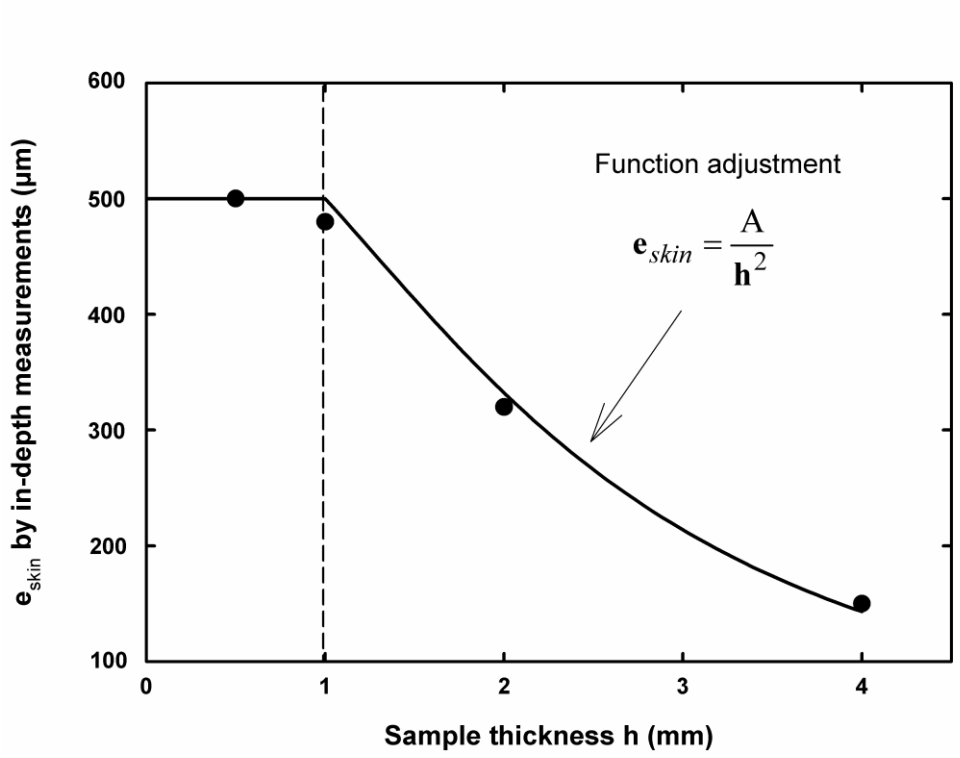

Figure 8 : Influence of the mold geometry on the skin thickness.